## Slicing Newton spheres with a two-camera 3D imaging system

Yasashri Ranathunga, Temitayo Olowolafe, Emmanuel Orunesajo, Hackim Musah, Suk Kyoung Lee and Wen Li\*

Department of Chemistry, Wayne State University, Detroit, MI, 48202, USA

\*wli@chem.wayne.edu

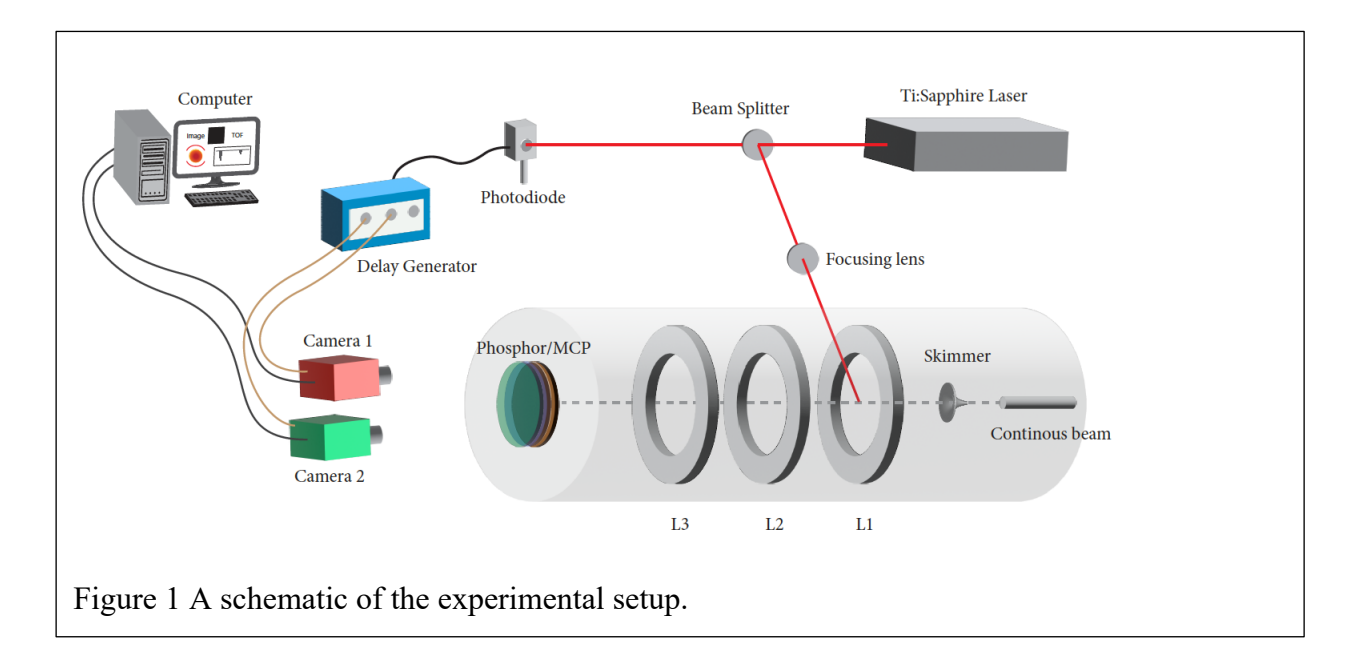
Abstract: We demonstrate a simple approach to achieve three-dimensional (3D) ion momentum imaging. The method employs two complementary metal-oxide semiconductor (CMOS) cameras in addition to a standard microchannel plates (MCP)/phosphor screen imaging detector. The two cameras are timed to measure the decay of luminescence excited by ion hits to extract the time of flight (TOF). The achieved time resolution is better than 10 nanoseconds, which is mainly limited by camera jitters. A better than 5 nanosecond resolution can be achieved when the jitter is suppressed.

Momentum imaging is a widely used technique for probing reaction dynamics, which include photodissociation, photoionization, and reactive/non-reactive scattering. This technique was initially implemented to measure the 2D momentum vectors of ions/electrons accelerated by either a homogenous¹ or an inhomogeneous electric field (velocity map imaging (VMI))² with a 2D imaging detector. The 3D momentum distributions are obtained either through a mathematical inversion method³-5 or the slice imaging technique⁴-8, in which a center slice of the 3D product Newton spheres was extracted. More recently, the technique has become 3D capable with time-and position-sensitive detectors⁴-1². 3D momentum imaging provides a complete characterization of the products' newton spheres and offers the most detailed information. However, existing 3D detectors have improved¹³-¹⁶ but still limited multi-hit capability compared to that of the 2D detection scheme and can lead to an extended data acquisition time. Pixelated detectors such as PImMS¹¹, ¹⁶ and Tpx3Cam¹⁶, ²⁰ avoid such a problem but they also have issues such as low spatial resolution and a high cost.

An interesting scheme for achieving 3D momentum imaging first demonstrated by Zajfman and coworkers<sup>21</sup> exploited the decay of the luminescence of the phosphor screen to extract the TOFs of particle hits. In this approach, with an image intensifier gated at a fixed time delay after the laser pulse, two cameras (one gated with the image intensifier) were used to measure the

relative brightness of the same events to retrieve the time of flight. This method can achieve high resolution (1 nanosecond temporal resolution and 50 µm spatial resolution) with great multi-hit capability. Over the years, a few different implementations based on the same principle have been developed by using a double exposure camera<sup>22</sup> or a fast frame camera (54 kHz)<sup>23</sup>. Here in this Communication, we show it has now become possible without specialized equipment such as gated image intensifiers or fast cameras, 3D imaging of particles can be achieved by using two regular CMOS cameras. The gating is implemented with the camera shutter function directly. Better than 10 nanoseconds temporal resolution can be obtained while a better resolution is also possible.

The experimental setup including the laser system, the vacuum chamber, and the VMI spectrometer is a standard 2D/3D VMI system, which has been described previously<sup>12, 24</sup> and a sketch is shown in Fig. 1. We will focus on the detection system, which comprises two CMOS cameras (Basler acA720-520um) in addition to a standard MCP/phosphor screen imaging detector (Photonis APD with 75 mm dia. dual MCPs and P47 phosphor) and a delay generator (DG535, Stanford Research System). The ions/electrons after being generated in the interaction region and accelerated by the VMI electric fields impact the MCPs and produce secondary electron avalanche which excites the phosphor. The brightness of the luminescence decays exponentially with a time constant, a characteristic of the type of phosphor used in the detector (for P47, the decay constant is ~50 ns). The two cameras sit side-by-side behind the phosphor screen and both are focused on the screen. The camera's shortest exposure time is 1 µs, which allows one to gate on a particular



mass when detecting ions. However, this is not short enough to gate the decay of the P47 phosphor, which decays to 1% of the highest brightness by 250 ns. Instead, we are utilizing the rising edge of the camera shutter to gate the luminescence. The delay generator triggered by a laser signal is used to delay this shutter opening right after the arrival of the slowest ions. The second camera's shutter is adjusted to open before the fastest ions arrive and stay open for about 30 µs. This guarantees that the second camera will capture the complete decay of the luminescence of all ions regardless of their TOFs.

The summed pixel intensity corresponding to an ion hit event in the second camera can be simply expressed by the following equation,

$$I_2 = \int_T^\infty I_0 \cdot e^{\frac{-(t-T)}{\tau}} dt = I_0 \tau \tag{1}$$

in which  $I_0$  is the initial brightness, T is the arrival time of the ion fragment, and  $\tau$  is the decay time constant of the phosphor. The summed pixel intensity of the same event in the first camera (gated) camera is

$$I_{1} = \int_{T'-T}^{T'+1} k \cdot I_{0} \cdot e^{\frac{-t}{\tau}} dt = k \cdot I_{0} \cdot \tau \left(-e^{-\frac{T'+1}{\tau}} + e^{\frac{T-T'}{\tau}}\right) = k \cdot I_{2} \cdot e^{\frac{T-T'}{\tau}}$$
(2)

in which T is the arrival time, T' is the gate opening time and T'+1 is the gate closing time with  $\mu$ s as their unit. Because  $\tau$  is significantly smaller than  $1 \mu$ s,  $e^{-\frac{T'+1}{\tau}}$  can be considered as zero and thus the third equal sign applies. k is the constant between the intensities of the same ion event viewed by the two cameras when both shutters are fully open, reflecting the difference in camera gain and light collection efficiency by the camera lenses, etc. The pixel intensity ratio between the two cameras  $(\Omega)$  is

$$\Omega = \frac{I_1}{I_2} = k \cdot e^{\frac{T - T'}{\tau}} \tag{3}$$

Therefore, the time of arrival of the ion is simply given by

$$T = \tau \ln \left(\frac{\Omega}{k}\right) + T' \tag{4}$$

This is a simple result that shows the TOFs can be retrieved from the ratio of the camera intensities. Note both k and T' can be combined into a constant  $C = -\ln k + T'$  and thus equation 4 can be further simplified to give

$$T = \tau \ln \Omega + C \tag{5}$$

 $\tau$  and C can be extracted from a calibration curve. This equation is different from that in Strasser et al.<sup>21</sup> because the gating schemes are different. It is possible to use the falling edge to gate the phosphor decay in our setup but the performance is not as good due to a worse jitter.

In the experiment, both cameras are triggered by the delay generator, which in turn is triggered by the laser at 1 kHz. The camera resolution is set at 260 pixels  $\times$  260 pixels. The images from both cameras are acquired by a desktop PC using USB3 interface. Each image is subjected to real-time analysis to locate clusters of non-zero pixels corresponding to particle hit events and center-of-mass calculations are performed on each cluster to give accurate positions  $(x,y)^{25}$ . The gray values of each pixel within the cluster are summed to give the total hit intensity. The intensity ratios and TOF calculations are done offline.

To validate and test the performance of the detection system, we produce ions by strong field ionization of methyl iodide (CH<sub>3</sub>I) using ultrashort 800 nm laser pulses (~30 fs) generated by a Ti:sapphire amplification system (KMLabs, Red Dragon, 1 kHz, 1 mJ). The laser intensity was estimated to be around 5×10<sup>13</sup> W/cm² at the focal spot. The ionization process can lead to both singly and multiply charged ions, which dissociate into various fragments such as CH<sub>3</sub>+, I<sup>+</sup> and I<sup>2+</sup>. The underlying dynamics have been investigated thoroughly in numerous previous studies<sup>26-29</sup>. The system is employed here to characterize the new technique. To achieve a high count rate to investigate the jitter issue and characterize the time resolution, we also carry out a photoemission experiment from a stainless disc mounted on the repeller of the VMI spectrometer. This is done in a newly built VMI apparatus designed for photoemission and photodesorption/ionization studies. The details of the apparatus will be described in a future publication but it is similar to the one employed previously<sup>30</sup>. The laser used is a Continuum Surelite II Nd:YAG laser. The third harmonic at 355 nm is used and the pulse duration is about 4 ns. The laser power is at 10 μJ/pulse.

We first use photoelectrons to validate equations 4 and 5 and to characterize the time resolution. The voltages on the VMI electrodes can be switched to detect ions, electrons, or both through pulsing<sup>31</sup>. The reason for using photoelectrons is because the spread of TOFs of electrons is short (full width <2 ns) under our VMI operating conditions and it offers a good benchmark for the time resolution. We also use a high count rate of ~40 electrons/shot. In the experiment, we vary the delay of the first camera trigger (T') to simulate a changing time of arrival and measure the relative brightness of each event. At each trigger delay, the  $\Omega$  values form a distribution and the peak  $\Omega$  value is taken as the  $\Omega$  for that trigger delay. Fig. 2a shows the plot between the camera trigger delay (T') and  $\ln \Omega$ . The linear relationship and the extracted  $\tau = 37$  ns verify the validity of equations 4 and 5 and offer a straightforward calibration method for  $\tau$ . The negative slope in the fitting reflects the fact that we are changing the camera trigger delay to simulate TOF change. They are related by the rearranged equation 4:

$$T' = -\tau \ln\left(\frac{\Omega}{k}\right) + T \tag{7}$$

For the ion experiment, the extracted  $\tau$  is 42 ns, suggesting a small variation of decay constants between different detectors and the necessity to do an in-situ calibration. With the fitted  $\tau$ , a TOF

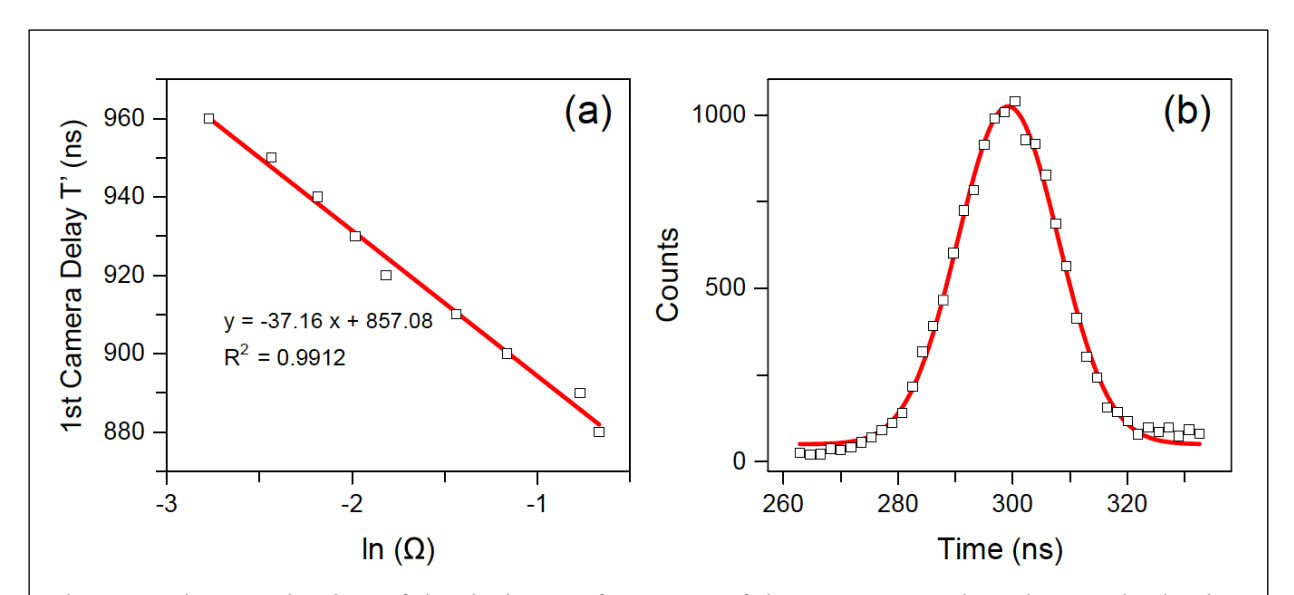


Figure 2 Characterization of the timing performance of the two-camera imaging method using photoelectrons. (a) Natural logarithm of pixel intensity ratio vs. the camera tigger delay. The red line is the linear fitting. (b) An electron TOF spectrum showing the time resolution of the system with a standard devision of 8.8 ns, derived from a gaussian fit (red curve).

spectrum can be constructed for any trigger delay. Note the intercept C value in equation 5 needs an additional calibration process but it is not done here because we focus on the TOF distributions instead of the absolute TOF value. An example of such a TOF spectrum is shown in Fig. 2b. This distribution can be fitted nicely with a Gaussian function with a full-width half maximum (FWHM) of 20.7 ns, which corresponds to a time resolution of 8.8 ns (the standard deviation). Note this value is convoluted with the TOF spread of electrons (Full width <2 ns) and the laser pulse duration (FWHM 4 ns). The true resolution will be slightly better. The leading factor for this resolution seems to be a jitter between the trigger and the actual shutter opening in the camera. This is confirmed by the fact that the peak  $\Omega$  value changes from shot to shot at the same trigger delay. We further quantify this using two tests in which we look into the TOF distributions within a single laser shot. Within the same camera frame, the frame-to-frame jitter should not play a role. In the first test, we select only the laser events with which the peak  $\Omega$  value falls into a particular range, and the resulting TOF distribution is shown in Fig. 3a. Here the FWHM significantly narrows down to 11.2 ns, corresponding to a standard deviation of 4.8 ns. In the second test, we plot the distributions of relative TOF, which is the difference between each TOF value and the peak TOF of each TOF distribution (converted from single-shot  $\Omega$  distributions). This is shown in Fig. 3b.

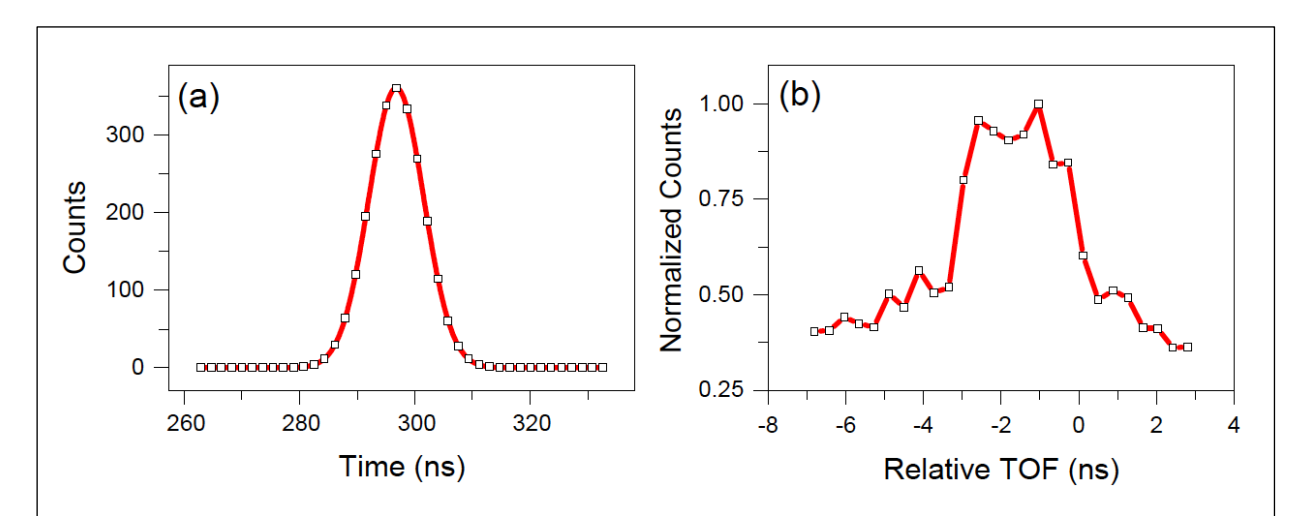


Figure 3 (a) An electron TOF spectrum when selecting camera frames with a similar time delay between the camaera trigger and the opening of the camera shutter. This suppresses trigger jitter and achieves a better TOF resolution of 4.8 ns (standard deviation) (b) A relative TOF spectrum by calculating the difference between each TOF value and the peak TOF value within the same camera frame. The width of the main feature is 3 ns.

The distribution is not Gaussian but the main feature is less than 3 ns wide. The non-gaussian shape could be due to further jitter among different pixels in the same camera frame. Both of these results suggest that the camera shutter jitter limits the achieved time resolution but it can be corrected. Furthermore, they also show that the rise time of the camera shutter is quite fast in just a few nanoseconds range, which is remarkable for such low-cost cameras. We tested one additional camera with a different sensor in the lab and found a similar shutter speed, suggesting such a performance might not be unique for a particular camera. On the other hand, multi-hits (tens to hundreds of ions) per shot are required to measure and correct the frame-to-frame jitter to improve time resolution. The ultimate time resolution also depends on the camera noise and how narrow is the intensity ratio distribution when both cameras are fully open (the k distribution). In our case, the 5% relative standard deviation ( $\sigma_k/k$ ) of the distribution poses a resolution limit of 2 ns with the P47 phosphor. This can be improved with a faster phosphor because the resolution scales linearly with the decay constant.

To test the real-world performance of the two-camera imaging system, we detect the CH<sub>3</sub><sup>+</sup> ions arising from strong field ionization of methyl iodide using the VMI apparatus. The average count rate is about 1 event/laser shot. A 2D VMI image is shown in Fig. 4a. In this image, the intense feature in the middle is from dissociative single ionization  $(CH_3I \rightarrow CH_3I^+ + e \rightarrow CH_3^+ +$ I). while the larger outside rings are from dissociative double ionization ( $CH_3I \rightarrow CH_3I^{2+} + 2e \rightarrow I$ ).  $CH_3^+ + I^+$ ). The double ring is due to the production of different electronic states of co-fragment I<sup>+</sup> cation<sup>12, 27</sup>. The energy separation between the two rings is ~0.8 eV. Thanks to the velocity focusing afforded by the VMI spectrometer, the momentum resolution is decent to resolve the two rings. However, with the additional TOF information for each ion obtained using the two-camera imaging system, we can apply a temporal slice of 10 ns to the same set of data that gives the unsliced image in Fig. 4a. The width (10 ns) is 1/10 of the total TOF spread of the methyl cation (~100 ns). Fig. 4b shows the sliced image. In this figure, the double ring is much better resolved and the effect of "crushing" is removed. Furthermore, we can slice at different TOF to reconstruct the full 3D Newton sphere, as shown in Fig. 4c. It is possible to stretch the Newton sphere more along the TOF axis to allow a "thinner" slice. However, the small decay constant of P47 limits the overall time range to be around 100 ns, and thus the full 3D momentum distribution will not be available, if stretched further. This can be addressed by using a slower decay phosphor such as P46 (decay constant ~250 ns). Additional cameras can be added to extend the range of detection

or to detect ions with different TOFs. A better time resolution could also be achieved if the camera jitter was suppressed. However, the vacuum chamber for the ion experiment was designed for coincidence measurements with a very dilute sample (double skimmed molecular beam), we are not able to achieve the needed count rate to suppress the camera jitter. Nonetheless, the demonstrated sub 10-ns resolution is sufficient for most ion imaging experiments.

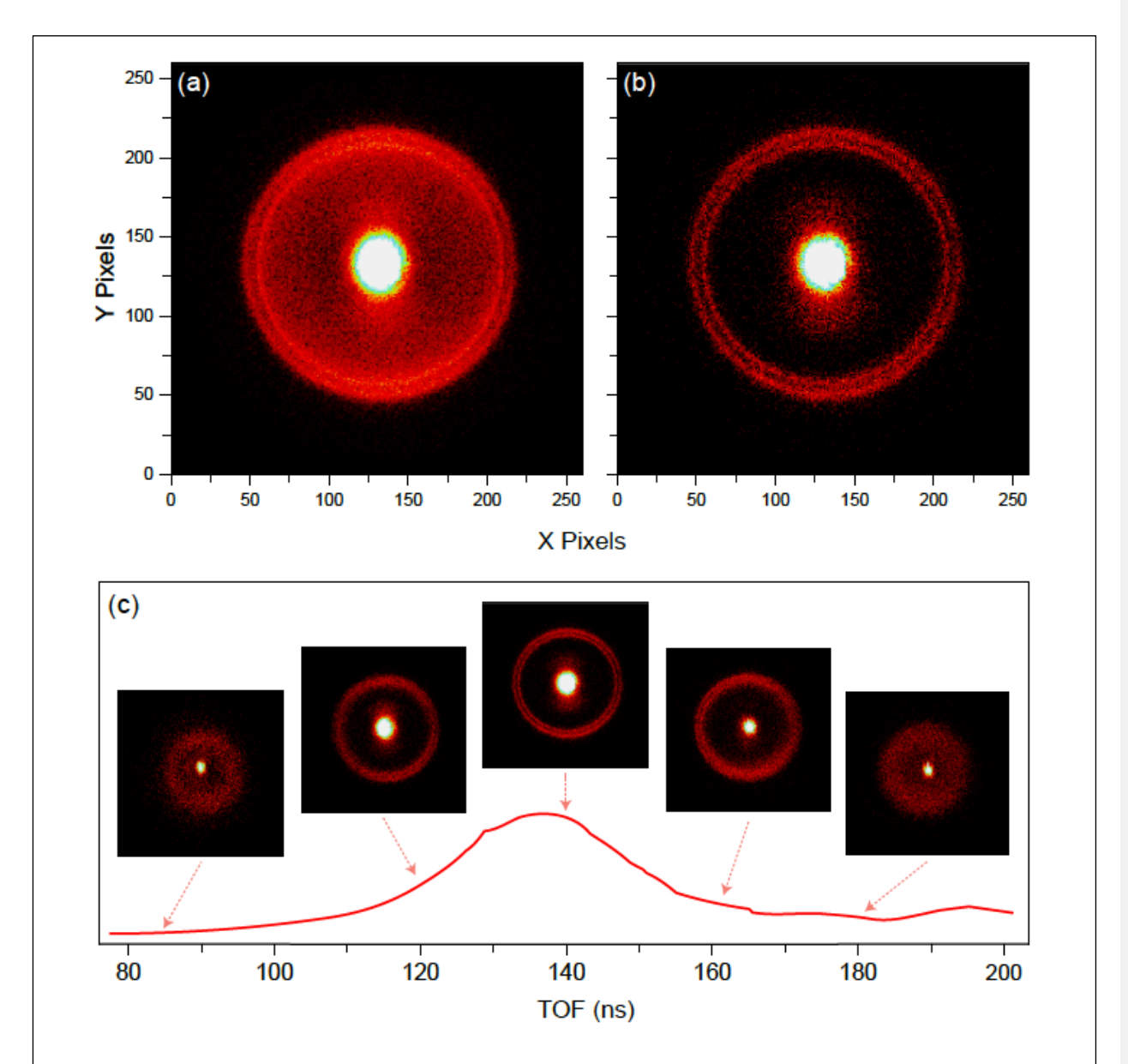


Figure 3 (a) A unsliced ("crushed") spatial image of methyl cation arising from strong field dissociative ionization of methyl iodide. (b) A sliced image of methyl cation obtained from the two-camera setup with a time slice width of 10 ns. (c) A few sliced images at different TOF with a temporal slice of 10 ns. They show the temporal evolution of the Newton sphere.

Deleted:

To summarize, without using specialized timing devices, gated image intensifiers, and fast frame cameras, we developed a simple two-camera 3D imaging method to achieve a sub-10 ns time resolution in measuring the time of flight of particles, which is sufficient for 3D and slice ion imaging. The technique is also well suited for detecting ions ejected from a material surface in a laser desorption/ionization process because each laser shot can produce tens or hundreds of ions and multi-hit capability becomes indispensable to achieve 3D imaging<sup>32</sup>. The technique should also be applicable for measuring photon arrival time when combined with an image intensifier with appropriate phosphor material. This will allow the technique to be used in wider applications such as wide-field fluorescence lifetime imaging (wf-FLIM)<sup>33-35</sup> and laser light detection and ranging (LIDAR). Due to the massive multi-hit capability, the detection rate can reach as high as ten million events per second. An extension to electron 3D momentum imaging requires at least one order of magnitude improvement in the time resolution<sup>36</sup>. From equation 5, the most effective way to achieve this is to use faster decay phosphors<sup>37, 38</sup>, provided that the camera jitter can be completely suppressed and the rising time of a shutter is short enough to gate the faster decay. This will be explored in future work.

## Acknowledgments

This material is based upon work supported by the National Science Foundation under Award No. CHE 2107860 (photoemission from surfaces) and the U.S. Department of Energy (DOE), Office of Science, Basic Energy Sciences (BES), under Award # DE-SC0020994 (strong field dissociative ionization of methyl iodide).

## References

- <sup>1</sup> D. W. Chandler, and P. L. Houston, J. Chem. Phys. **87** (1987) 1445.
- <sup>2</sup> A. Eppink, and D. Parker, Rev. Sci. Instrum. **68** (1997) 3477.
- <sup>3</sup> L. A. Shepp, and B. F. Logan, IEEE Transactions on Nuclear Science **21** (1974) 21.
- <sup>4</sup>R. N. Strickland, and D. W. Chandler, Appl. Opt. **30** (1991) 1811.
- <sup>5</sup> J. O. F. Thompson *et al.*, J. Chem. Phys. **147** (2017) 074201.
- <sup>6</sup>D. Townsend, M. Minitti, and A. Suits, Rev. Sci. Instrum. **74** (2003) 2530.
- <sup>7</sup> J. J. Lin *et al.*, Rev. Sci. Instrum. **74** (2003) 2495.
- <sup>8</sup> C. R. Gebhardt et al., Rev. Sci. Instrum. **72** (2001) 3848.

- <sup>9</sup> G. Basnayake et al., J. Phys. B-At. Mol. Opt. Phys. **55** (2022) 023001.
- <sup>10</sup> M. Takahashi, J. P. Cave, and J. H. D. Eland, Rev. Sci. Instrum. **71** (2000) 1337.
- <sup>11</sup> J. Ullrich et al., Rep. Prog. Phys. **66** (2003) 1463.
- <sup>12</sup> S. K. Lee *et al.*, Rev. Sci. Instrum. **85** (2014) 123303.
- <sup>13</sup> C. Weeraratna *et al.*, J. Chem. Phys. **149** (2018) 084202.
- <sup>14</sup> Y. F. Lin *et al.*, Rev. Sci. Instrum. **86** (2015) 096110.
- <sup>15</sup> R. Wallauer *et al.*, Rev. Sci. Instrum. **83** (2012) 103905.
- <sup>16</sup> K. A. Hanold et al., Rev. Sci. Instrum. **70** (1999) 2268.
- <sup>17</sup> A. Nomerotski *et al.*, J. Instrum. **5** (2010) C07007.
- <sup>18</sup> A. T. Clark et al., J. Phys. Chem. A **116** (2012) 10897.
- <sup>19</sup> A. Zhao *et al.*, Rev. Sci. Instrum. **88** (2017) 113104.
- <sup>20</sup> D. A. Debrah et al., Rev. Sci. Instrum. **91** (2020) 023316.
- <sup>21</sup> D. Strasser et al., Rev. Sci. Instrum. **71** (2000) 3092.
- <sup>22</sup> L. Dinu *et al.*, Rev. Sci. Instrum. **73** (2002) 4206.
- <sup>23</sup> L. M. Hirvonen *et al.*, New J. Phys. **17** (2015) 023032.
- <sup>24</sup> Q. Liao et al., Phys. Rev. A **96** (2017) 023401.
- <sup>25</sup> W. Li *et al.*, Rev. Sci. Instrum. **76** (2005) 063106.
- <sup>26</sup> H. Liu et al., J. Chem. Phys. **126** (2007) 044316.
- <sup>27</sup> M. E. Corrales et al., J. Phys. Chem. A **116** (2011) 2669.
- $^{28}\,\mathrm{Y}.$  Wang et al., J. Phys. Chem. A 112 (2008) 3846.
- <sup>29</sup> A. H. Winney *et al.*, J. Phys. Chem. Lett. **9** (2018) 2539.
- $^{30}\,\mathrm{L}.$  Fan et al., J. Phys. Chem. Lett. 9 (2018) 1485.
- <sup>31</sup> L. Fan *et al.*, J. Chem. Phys. **147** (2017) 013920.
- $^{32}\,{\rm G.}$  A. Stewart et~al., J. Phys. Chem. C  $\bf 126~(2022)~17135.$
- <sup>33</sup> G. Marriott *et al.*, Biophysical Journal **60** (1991) 1374.
- <sup>34</sup> G. Vereb *et al.*, Biophysical Journal **74** (1998) 2210.
- <sup>35</sup> N. Sergent *et al.*, Opt. Express **18** (2010) 25292.
- <sup>36</sup> S. K. Lee *et al.*, J. Chem. Phys. **141** (2014) 221101.
- <sup>37</sup> B. Winter *et al.*, Rev. Sci. Instrum. **85** (2014) 023306.
- <sup>38</sup> E. Orunesajo *et al.*, J. Phys. Chem. A **125** (2021) 5220.